Journal of Materials Chemistry B

PAPER

View Article Online
View Journal | View Issue

Cite this: J. Mater. Chem. B, 2014, 2, 231

Light-up bioprobe with aggregation-induced emission characteristics for real-time apoptosis imaging in target cancer cells†

Dan Ding,[a] Jing Liang,[a] Haibin Shi,[a] Ryan T. K. Kwok,[b] Meng Gao,[c] Guangxue Feng,[a] Youyong Yuan,[a] Ben Zhong Tang*[bd] and Bin Liu*[ac]

Received 23rd October 2013
Accepted 24th October 2013

DOI: 10.1039/c3tb21495h

www.rsc.org/MaterialsB

Specific bioprobes that are capable of real-time and targeted monitoring and imaging of cancer cell apoptosis are highly desirable for cancer diagnosis and the evaluation of cancer therapy efficacy. In this work, an asymmetric fluorescent light-up bioprobe with aggregation-induced emission (AIE) characteristics was designed and synthesized by the conjugation of two different hydrophilic peptides, caspase-specific Asp-Glu-Val-Asp (DEVD) and cyclic Arg-Gly-Asp (cRGD), onto a typical AIE luminogen of a tetraphenylsilole (TPS) unit. The asymmetric probe is almost non-emissive in aqueous solution and its fluorescence is significantly switched on in the presence of caspase-3. The fluorescence turn-on is due to the cleavage of the DEVD moiety by caspase-3, and the aggregation of released TPS-cRGD residues, which restricts the intramolecular rotations of TPS phenyl rings and populates the radiative decay channels. Application of the asymmetric light-up probe for real-time targeted imaging of cancer cell apoptosis is successfully demonstrated using integrin $\alpha_v\beta_3$ receptor overexpressing U87MG human glioblastoma cells as an example. The probe shows specific targeting capability to U87MG cancer cells by virtue of the efficient binding between cRGD and integrin $\alpha_v\beta_3$ receptors and is able to real-time monitor and image cancer cell apoptosis in a specific and sensitive manner.

1 Introduction

Apoptosis is a mode of programmed cell death in multicellular organisms.[1] As the deregulation of apoptosis can cause cancer and responses to anticancer therapeutics, real-time apoptosis imaging at single cancer cellular level will open up new opportunities in the early prognosis of cancers, tracing of the cancer progress, as well as the efficacy estimation of new anticancer agents.[2] Recently, specific probes for the identification of target cancer cells among various cancer cell lines or against normal cells have attracted increasing interest in fundamental biological studies and clinical diagnosis.[3] Therefore, real-time apoptosis imaging in target cancer cells is of great importance in offering scientists with sight and insight into specific cancer developments and to provide assessment of the anticancer activities of clinically available molecular-targeted drugs. Additionally, the high accumulation of apoptosis-monitoring probes in target cancer cells also minimizes the possible toxic side effects and false positive signals. As a consequence, effective and sensitive probes with the capability of real-time apoptosis imaging in target cancer cells are in urgent pursuit. To date, there have been several strategies for detecting apoptosis at cellular level.[4–10] Among them, the monitoring of cytosolic caspases, which are a family of cysteine proteases and specific apoptotic mediators, has been demonstrated to be a very effective strategy to evaluate apoptosis.[2c,5–10] These probes are generally composed of caspase-specific peptide substrates and fluorescent/bioluminescent units including latent fluorophores,[5] fluorescent proteins,[6] fluorescence resonance energy transfer pairs,[7] donor/quencher pairs,[8] D-lucferin or luciferase.[9] These fluorescent/bioluminescent units respond to cell apoptosis upon peptide substrate cleavage by caspases. Although these methods have enabled the detection of caspase activity at the cellular level, they often require a complicated probe design, and suffer from one or more disadvantages, such as poor cell permeability, aggregation caused quenching (ACQ), high background signal, or small fluorescence/bioluminescence signal changes. More importantly, very few probes have been reported for apoptosis imaging in target cancer cells, which are all limited to nanoparticle based systems.[10]

[a]Department of Chemical and Biomolecular Engineering, National University of Singapore, 117576, Singapore. E-mail: cheliub@nus.edu.sg; Fax: +65 67791936; Tel: +65 65168049

[b]Department of Chemistry and Division of Biomedical Engineering, Hong Kong University of Science and Technology, Clear Water Bay, Kowloon, Hong Kong, China. E-mail: tangbenz@ust.hk

[c]Institute of Materials Research and Engineering, 3 Research Link, 117602, Singapore

[d]SCUT–HKUST Joint Research Laboratory, Guangdong Innovative Research Team, State Key Laboratory of Luminescent Materials and Devices, South China University of Technology, Guangzhou, 510640, China

† Electronic supplementary information (ESI) available. See DOI: 10.1039/c3tb21495h

Exploration of new probe designs is highly desirable for real-time apoptosis monitoring in target cancer cells, which will provide a useful tool for cancer diagnosis and the evaluation of cancer therapy efficacy.

Recently, we have developed a novel class of organic luminogens with a unique aggregation-induced emission (AIE) signature, which is exactly opposite to the ACQ effect for conventional fluorophores.[11] The AIE luminogens generally have rotating units (*e.g.* phenyl rings) to promote fast discrete diffusion. In dilute solutions, the AIE luminogens are non-emissive and in a "turn-off" state due to the fast non-radiative decay of the excited states arising from the low-frequency motions of rotating units. In aggregates, the AIE luminogens luminesce intensively with fluorescence "turn-on" *via* a mechanism of the restriction of intramolecular rotations (RIR).[12] By virtue of the AIE phemomenon, the luminogens with AIE characteristics are attracting increasing attention and have been widely used for sensing and imaging applications.[13] Most recently, we have developed AIE luminogen based light-up probes, which have been successfully used for intracellular protein monitoring *in vitro*.[14] The successful light-up probe design strategy has motivated us to explore new specific bioprobes with AIE characteristics for apoptosis imaging in target cancer cells.

In this contribution, we designed and synthesized a light-up molecular probe with an AIE signature for real-time apoptosis imaging in target cancer cells. Two different peptide sequences, cyclic Arg-Gly-Asp (cRGD) and the acetyl protective N-terminal Asp-Glu-Val-Asp (Ac-DEVD), were conjugated to each side of the tetraphenylsilole (TPS) unit to afford the asymmetric bioprobe of Ac-DEVD-TPS-cRGD (Scheme 1). cRGD and Ac-DEVD peptides were selected as the biorecognition units because cRGD shows high affinity to integrin $\alpha_v\beta_3$ receptors that are overexpressed in many cancer cells[15] and Ac-DEVD is a peptide substrate that can be specifically cleaved by caspases-3/7.[16] We further demonstrated that the asymmetric AIE bioprobe shows both targeting ability to integrin $\alpha_v\beta_3$ receptor overexpressing cancer cells and the specific capability of real-time apoptosis sensing and imaging in live cancer cells with high sensitivity. As compared to our previous light-up bioprobes, the special asymmetric probe design is not only able to detect and image live cancer cell-specific apoptosis, but also achieve improved sensitivity by providing a low background signal.

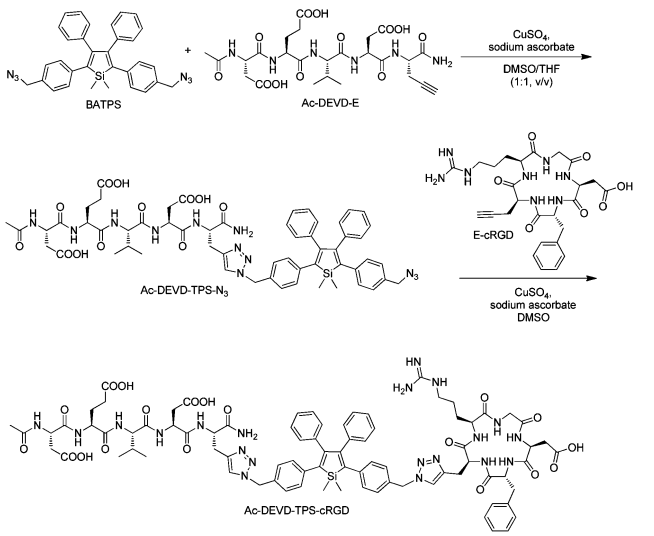

Scheme 1 Synthetic route to Ac-DEVD-TPS-cRGD.

2 Experimental

2.1 Materials

The ethylyne-functionalized cyclic RGD (E-cRGD) and the ethylyne-functionalized acetyl protective N-terminal Asp-Glu-Val-Asp (Ac-DEVD-E) were purchased from GL Biochem Ltd. Cathepsin B, lysozyme, pepsin, papsin, trypsin, bovine serum albumin (BSA), copper(II) sulfate, sodium ascorbate, dimethyl sulfoxide (DMSO), piperazine-*N*,*N*′-bis(2-ethanesulfonic acid) (PIPES), trifluoroacetic acid (TFA), penicillin–streptomycin solution, trypsin-ethylenediaminetetraacetic acid (EDTA) solution and 3-(4,5-dimethylthiazol-2-yl)-2,5-diphenyl tetrazolium bromide (MTT) were all purchased from Sigma-Aldrich. Recombinant human caspase-3, caspase-7 and caspase-1 were customized from R&D Systems. Annexin V-Alexa Fluor 488 was purchased from Invitrogen. Staurosporine (STS) was purchased from Biovision. Caspase inhibitor 5-[(*S*)-(+)-2-(methoxymethyl)-pyrrolidino]sulfonylisatin was provided by Calbiochem. Cleaved caspase-3 (Asp175) (5A1E) Rabbit mAb (#9664) was purchased from Cell Signaling. Mouse anti-rabbit IgG-TR (sc-3917) was customized from Santa Cruz. Fetal bovine serum (FBS) was provided by Gibco (Lige Technologies, Switzerland). Tetrahydrofuran (THF) was distilled from sodium benzophenone ketyl under dry nitrogen immediately prior to use. Milli-Q water was supplied by a Milli-Q Plus System (Millipore Corporation, Bedford, USA). U87MG human glioblastoma cell line, MCF-7 human breast cancer cell line and 293 T normal cell line were provided by American Type Culture Collection. The bisazido-functionalized tetraphenylsilole (BATPS) was synthesized according to the literature.[14a]

2.2 Characterization

^{1}H and ^{13}C NMR spectra were measured on a Bruker ARX 600 NMR spectrometer. Chemical shifts were reported in parts per million (ppm) referenced with respect to residual solvent ($(CD_3)_2SO$ = 2.50 ppm or tetramethylsilane $Si(CH_3)_4$ = 0 ppm). The synthesized samples were purified by preparative high pressure liquid chromatography (HPLC) (Agilent 1100 series). The analytical LC profiles and molecular mass were acquired using liquid chromatography-ion trap-time-of-flight mass spectrometry (LCMS-IT-TOF) (Shimadzu). 0.1% TFA/H_2O and 0.1% TFA/acetonitrile were used as eluents for all HPLC experiments. The column used for the preparative HPLC was ZORBAX SB-C18, 5 μm (Agilent) with the following flow parameters: flow rate = 2 mL min^{-1}, 0 min: 20% ACN, 8 min: 50% ACN, 15 min: 100% ACN. The column used for the analytical HPLC was Luna 5μ C18(2) (Phenomenex®) with the following flow parameters: flow rate = 0.6 mL min^{-1}; 10–100% ACN from

0.01 min to 13 min. UV-vis absorption spectra were recorded on a Shimadzu UV-1700 spectrometer. Photoluminescence (PL) spectra were recorded on a Perkin-Elmer LS 55 spectrofluorometer. All PL spectra were measured with an excitation wavelength of 360 nm. The average particle size and size distribution of the samples were measured by laser light scattering (LLS) with a particle size analyzer (90 Plus, Brookhaven Instruments Co. USA) at a fixed angle of 90° at room temperature.

2.3 Synthesis, purification and characterization of Ac-DEVD-TPS-N_3

Excess amounts of BATPS (40 mg, 75 μmol) and Ac-DEVD-E (9.2 mg, 15 μmol) were dissolved in 0.8 mL of a DMSO and THF mixture (v/v = 1 : 1). The mixture was sonicated to obtain a clear solution. A click reaction was initiated by the subsequent addition of 0.2 mL of an aqueous solution containing $CuSO_4$ (1.2 mg, 7.5 μmol) and sodium ascorbate (3 mg, 15 μmol). The reaction was constantly monitored by HPLC to maximize the formation of Ac-DEVD-TPS-N_3 and minimize the byproduct of Ac-DEVD-TPS-DVED-Ac by shaking at low temperature (4 °C) for a short period (12 h). The desired product of Ac-DEVD-TPS-N_3 was then purified by HPLC to yield Ac-DEVD-TPS-N_3 (5.1 mg, 30% yield) as a fine powder before further characterization by ^{1}H and ^{13}C NMR as well as LC-MS. ^{1}H NMR (DMSO-d_6, 600 MHz): δ 12.14 (br s, 3H), 8.13 (d, J = 7.2 Hz, 1H), 8.07 (d, J = 7.2 Hz, 1H), 7.89 (d, J = 8.4 Hz, 1H), 7.85 (d, J = 7.2 Hz, 1H), 7.72 (s, 1H), 7.57 (d, J = 8.4 Hz, 1H), 7.07 (s, 1H), 7.02–6.99 (m, 3H), 6.90–6.87 (m, 8H), 6.78–6.72 (m, 5H), 6.66–6.65 (m, 3H), 5.31 (s, 2H), 4.43–4.36 (m, 2H), 4.23 (s, 2H), 4.17–4.13 (m, 1H), 3.99–3.96 (m, 1H), 2.98–2.94 (m, 1H), 2.79–2.75 (m, 1H), 2.56–2.50 (m, 2H), 2.42–2.33 (m, 2H), 2.13–2.05 (m, 2H), 1.96 (s, 3H), 1.85–1.75 (m, 2H), 1.65–1.59 (m, 1H), 0.64 (d, J = 6.0 Hz, 6H); ^{13}C NMR (DMSO-d_6, 150 MHz): δ 206.4, 174.0, 172.2, 171.8, 171.6, 171.0, 170.9, 170.9, 170.1, 169.4, 153.8, 153.8, 143.2, 140.8, 140.7, 138.9, 138.7, 138.3, 138.3, 133.5, 132.9, 129.3, 129.2, 128.5, 128.1, 127.5, 127.5, 127.3, 126.4, 126.4, 126.4, 123.1, 57.7, 53.3, 52.4, 52.0, 51.1, 49.7, 49.5, 40.0, 39.9, 39.8, 39.7, 39.6, 39.5, 39.3, 39.2, 39.0, 35.9, 35.6, 30.6, 30.3, 29.9, 27.8, 26.9, 22.4, 20.4, 19.0, 17.9. IT-TOF-MS: m/z $[M + H]^+$ calc. 1137.46, found 1137.45.

2.4 Synthesis, purification and characterization of Ac-DEVD-TPS-cRGD

The purified Ac-DEVD-TPS-N_3 (5 mg, 4.4 μmol) and E-cRGD (3.7 mg, 6.5 μmol) were dissolved in 0.5 mL of DMSO. $CuSO_4$ (0.35 mg, 2.2 μmol) and sodium ascorbate (0.88 mg, 4.4 μmol) dissolved in 0.1 mL of water were added to the mixture to initiate the click chemistry. The reaction was allowed to proceed at room temperature under shaking for 2 days. The obtained product was purified by HPLC to yield Ac-DEVD-TPS-cRGD (4.5 mg, 60% yield) as a fine powder before further characterization with ^{1}H and ^{13}C NMR as well as LC-MS. ^{1}H NMR (DMSO-d_6, 600 MHz): δ 12.15 (br s, 6H), 8.17–8.14 (m, 2H), 8.08 (d, J = 7.8 Hz, 1H), 8.00 (d, J = 7.8 Hz, 1H), 7.92 (d, J = 7.2 Hz, 1H), 7.89 (d, J = 8.4 Hz, 1H), 7.86 (d, J = 7.8 Hz, 2H), 7.81 (d, J = 8.4 Hz, 1H), 7.74 (s, 1H), 7.69 (s, 1H), 7.58 (d, J = 7.8 Hz, 1H), 7.34 (t, J = 5.4 Hz, 1H), 7.08–7.02 (m, 6H), 6.95 (d, J = 7.2 Hz, 2H), 6.92–6.87 (m, 6H), 6.76–6.74 (m, 3H), 6.66–6.63 (m, 3H), 5.34 (s, 2H), 5.32 (s, 2H), 4.53–4.49 (m, 1H), 4.45–4.33 (m, 3H), 4.30–4.22 (m, 2H), 4.19–4.16 (m, 1H), 4.02–3.95 (m, 3H), 3.17–3.14 (m, 2H), 3.00–2.96 (m, 4H), 2.90–2.87 (m, 2H), 2.81–2.77 (m, 4H), 2.61–2.52 (m, 4H), 2.45–2.35 (m, 2H), 2.27–2.23 (m, 2H), 2.13–2.08 (m, 2H), 1.83–1.80 (m, 2H), 1.72 (s, 3H), 1.66–1.63 (m, 2H), 1.41–1.38 (m, 2H), 1.30–1.22 (m, 2H), 0.67 (d, J = 6.0 Hz, 6H), 0.66 (s, 6H). ^{13}C NMR (DMSO-d_6, 100 MHz): δ 174.0, 172.2, 171.8, 171.6, 171.5, 171.1, 170.9, 170.8, 170.6, 170.0, 169.5, 169.3, 156.6, 153.9, 153.9, 143.2, 142.8, 140.7, 140.6, 138.7, 138.3, 137.2, 133.5, 133.4, 129.2, 128.9, 128.49, 127.9, 127.5, 127.3, 127.2, 126.4, 126.1, 123.1, 123.1, 57.8, 54.3, 53.7, 52.4, 52.3, 52.1, 49.7, 49.6, 48.9, 43.1, 36.7, 35.9, 35.6, 35.1, 30.3, 30.0, 28.1, 27.9, 26.9, 25.0, 22.4, 19.0, 17.9, −4.2. IT-TOF-MS: m/z $[M + 2H]^{2+}$ calc. 854.36, found 854.85.

2.5 Enzymatic assays

In general, 2 μL of Ac-DEVD-TPS-N_3 or Ac-DEVD-TPS-cRGD in DMSO solution (1 mM) was first diluted with 50 μL of caspase-3 assay PIPES buffer (50 mM PIPES, 100 mM NaCl, 1 mM EDTA, 0.1% w/v CHAPS, 25% w/v sucrose, pH = 7.2), which was followed by the addition of a predetermined amount of the recombinant caspase-3 (40 ng μL^{-1} stock solution in assay buffer). The reaction mixture was incubated at 37 °C for 30 min, and was subsequently diluted to a total of 600 μL with Milli-Q water for PL measurements upon excitation at 360 nm.

2.6 Cell culture

U87MG human glioblastoma cells, MCF-7 human breast cancer cells and 293 T normal cells were cultured in Dulbecco's Modified Eagle's Medium (DMEM) containing 10% FBS and 1% penicillin-streptomycin at 37 °C in a humidified environment containing 5% CO_2, respectively. Before the experiments, the cells were pre-cultured until confluence was reached.

2.7 Apoptosis imaging in target cancer cells

U87MG glioblastoma cells were cultured in confocal imaging chambers (LAB-TEK, Chambered Coverglass System) at 37 °C. After 80% confluence, the medium was removed and the adherent cells were washed twice with 1 × PBS buffer. The Ac-DEVD-TPS-N_3 and Ac-DEVD-TPS-cRGD in FBS-free DMEM medium at a concentration of 5 μM were then added to the chamber, respectively. After incubation at 37 °C for 2 h, the cells were washed three times with 1 × PBS buffer and then incubated with staurosporine (STS, 1 μM) in FBS-free DMEM medium for 1 h to induce cell apoptosis. The cell monolayer was then imaged by confocal laser scanning microscope (CLSM, Zeiss LSM 410, Jena, Germany) with imaging software (Olympus Fluoview FV1000). For all the images, the confocal set up remained the same, *e.g.* the pinhole was set at 145 μm (60×) and the gain was set at 1. The fluorescent signals from the probes were collected upon excitation at 405 nm (1 mW) with a 505 nm longpass barrier filter. MCF-7 breast cancer cells and 293 T normal cells incubated with Ac-DEVD-TPS-cRGD, respectively,

were also studied following the same procedures. To study the competitive effect of free cRGD peptide on the cellular uptake of Ac-DEVD-TPS-cRGD, the U87MG cells were first incubated with 10 μM free cRGD in DMEM medium, which was followed by incubation with Ac-DEVD-TPS-cRGD in DMEM medium at 37 °C for 2 h before STS was used to induce cell apoptosis.

2.8 Co-localization studies

For co-localization with Annexin V-Alexa Fluor 488, the Ac-DEVD-TPS-cRGD-treated apoptotic U87MG cells were further incubated with a mixture of Annexin V-Alexa Fluor 488/FBS-free DMEM (v/v = 1 : 799) for 20 min at room temperature, which was followed by washing twice with 1 × PBS buffer. The cells were then kept in fresh FBS-free DMEM for CLSM imaging. For co-localization with active caspase-3 antibody, the Ac-DEVD-TPS-cRGD-treated apoptotic U87MG cells were first fixed with 3.7% formaldehyde in 1 × PBS for 30 min at room temperature. After washing twice with 1 × PBS, and being permeabilized with 0.1% Triton X-100 in 1 × PBS for 15 min, the cells were subsequently blocked with 2% BSA in 1 × PBS for 30 min and washed twice with 1 × PBS. Subsequently, the cells were further incubated with a mixture of cleaved caspase-3 primary antibody/1 × PBS (v/v = 1 : 99) for 2 h at room temperature. After washing twice with 1 × PBS buffer and then incubating with mouse anti-rabbit IgG-TR (0.8 μg mL^{-1}) in 1 × PBS for 4 h, the cells were washed twice with 1 × PBS before the cell monolayer was imaged by CLSM.

2.9 Real-time imaging of cancer cell apoptosis

U87MG glioblastoma cells were cultured in confocal imaging chambers at 37 °C. After 80% confluence, 5 μM Ac-DEVD-TPS-cRGD in FBS-free DMEM medium was added to the chamber. After incubation at 37 °C for 2 h, the cells were washed three times with 1 × PBS buffer. Subsequently, the confocal imaging chambers were placed on the CLSM platform, which was followed by the addition of STS (1 μM) in FBS-free DMEM medium. The cell monolayer was then imaged immediately by CLSM at the designated time intervals. All the images were taken under the same imaging conditions with excitation at 405 nm and a 505 nm longpass barrier filter.

2.10 Cytotoxicity study

The cytotoxicities of Ac-DEVD-TPS-N_3 and Ac-DEVD-TPS-cRGD against U87MG glioblastoma cells were evaluated by MTT assay. Briefly, U87MG cells were seeded in 96-well plates (Costar, IL, USA) at an intensity of 4×10^4 cells per mL. After 24 h incubation, the cells were exposed to a series of doses of Ac-DEVD-TPS-N_3 or Ac-DEVD-TPS-cRGD at 37 °C. After 48 h incubation, the wells were washed twice with 1 × PBS and 100 μL of freshly prepared MTT (0.5 mg mL^{-1}) solution in culture medium was added into each well. The MTT medium solution was carefully removed after 3 h incubation in the incubator. DMSO (100 μL) was then added into each well and the plate was gently shaken for 10 minutes at room temperature to dissolve all the precipitates that had formed. The absorbance of MTT at 570 nm was monitored by the microplate reader (Genios Tecan). Cell viability was expressed by the ratio of absorbance of the cells incubated with the sample suspension to that of the cells incubated with culture medium only.

3 Results and discussion

The acetyl protective N-terminal Asp-Glu-Val-Asp-TPS-azide probe (Ac-DEVD-TPS-N_3) was first synthesized in a 30% yield by a copper-catalyzed "click" reaction between a bisazido (BA)-functionalized TPS (BATPS) and an ethylyne (E)-functionalized Ac-DEVD (Ac-DEVD-E) in a DMSO–THF (v/v = 1 : 1) mixture. Afterwards the Ac-DEVD-TPS-N_3 was purified by HPLC and characterized with ^1H and ^{13}C NMR and LC-MS (Fig. S1 and S2 in the ESI†), further coupling between Ac-DEVD-TPS-N_3 and E-bearing cyclic RGD (E-cRGD) by click chemistry yielded Ac-DEVD-TPS-cRGD with a 60% yield. The purity and identity of the Ac-DEVD-TPS-cRGD were also confirmed by ^1H and ^{13}C NMR and LC-MS (Fig. S3 and S4 in the ESI†).

BATPS, Ac-DEVD-TPS-N_3 and Ac-DEVD-TPS-cRGD exhibit similar UV-vis absorption spectra in a DMSO–water (v/v = 1/199) mixture with a peak centered at 360 nm (Fig. S5 in ESI†). The photoluminescence (PL) spectra are shown in Fig. 1A. BATPS shows high fluorescence in a DMSO–water (v/v = 1/199) mixture with a quantum yield (Φ) of 0.17, measured using quinine sulfate in 0.1 M H_2SO_4 as the standard.[17] In comparison, Ac-DEVD-TPS-N_3 is weakly fluorescent ($\Phi = 0.01$) and Ac-DEVD-TPS-cRGD is almost non-emissive ($\Phi = 0.001$) in the same medium. The high fluorescence of BATPS is because the hydrophobic BATPS molecules form nanoaggregates in aqueous medium with an average size of ~95 nm measured by laser light scattering (LLS) and atomic force microscopy (AFM) (Fig. S6 in the ESI†). The conjugation of the Ac-DEVD peptide with TPS, however, leads to Ac-DEVD-TPS-N_3 with improved water-solubility relative to that of BATPS. Further coupling of the cRGD peptide endows the Ac-DEVD-TPS-cRGD with good water-solubility, which is further confirmed by the undetectable LLS signal. The high brightness for the BATPS aggregates and the almost zero fluorescence for the Ac-DEVD-TPS-cRGD molecular probe agree with the AIE mechanism. Due to the propeller-shaped structure of TPS,[12] the dynamic rotations of the phenyl rings non-radiatively deactivated their excited states in solution; in the aggregate state, the RIR opens the radiative decay channel. The extremely low background fluorescence signal makes the Ac-DEVD-TPS-cRGD probe promising to serve as an effective light-up probe with high sensitivity.

The principle of the probe Ac-DEVD-TPS-cRGD for apoptosis imaging in target cancer cells is illustrated in Scheme 2. By virtue of the specific binding between cRGD peptide and integrin $\alpha_v\beta_3$ receptors, the Ac-DEVD-TPS-cRGD should be favorably internalized by integrin $\alpha_v\beta_3$ receptor-overexpressed cancer cells over other cells with low receptor expression on the cell membrane. As Ac-DEVD-TPS-cRGD is highly water-soluble and shows almost no fluorescence in aqueous solution, it is hypothesized that the intracellular Ac-DEVD-TPS-cRGD internalized by healthy cancer cells without apoptosis can still

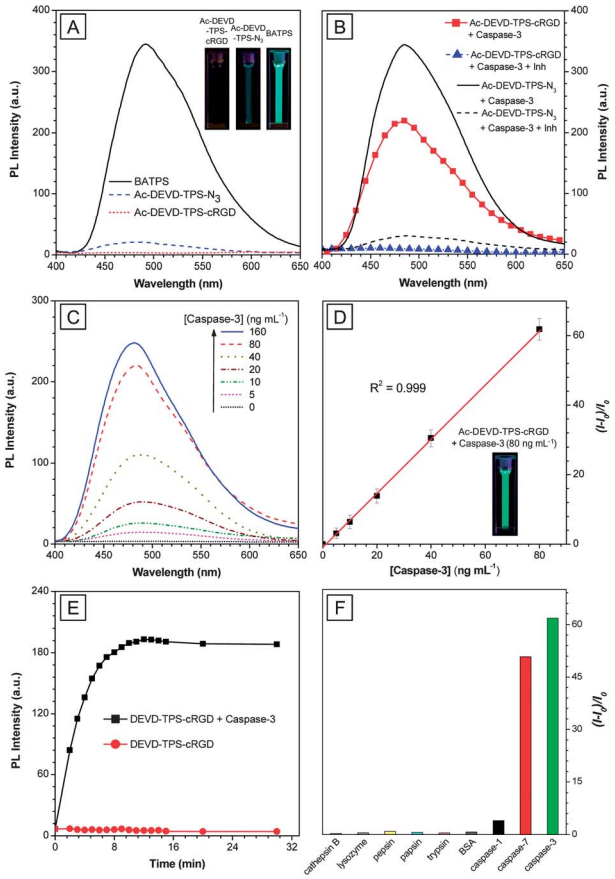

Fig. 1 (A) Photoluminescence (PL) spectra of BATPS, Ac-DEVD-TPS-N_3 and Ac-DEVD-TPS-cRGD in DMSO–water (v/v = 1 : 199). Inset: the corresponding photographs taken under illumination of a UV lamp. (B) PL spectra of Ac-DEVD-TPS-N_3 and Ac-DEVD-TPS-cRGD upon treatment with caspase-3 in the presence and absence of caspase-3 inhibitor (Inh). (C) PL spectra of Ac-DEVD-TPS-cRGD treated with various amounts of caspase-3 in PIPEs buffer at 37 °C for 30 min. (D) Plot of $(I - I_0)/I_0$ *versus* the caspase-3 concentration in PIPEs buffer. I and I_0 are the PL intensities of the assay in the presence and absence of caspase-3, respectively. Inset: the photograph taken under illumination of a UV lamp for Ac-DEVD-TPS-cRGD upon treatment with 80 ng mL^{-1} of caspase-3 for 30 min. (E) PL intensity changes of Ac-DEVD-TPS-cRGD upon incubation with and without caspase-3 from 0 to 30 min. (F) Plot of $(I - I_0)/I_0$ *versus* a variety of proteins, where I and I_0 are the PL intensities at protein concentrations of 80 and 0 ng mL^{-1}, respectively. [BATPS] = [Ac-DEVD-TPS-N_3] = [Ac-DEVD-TPS-cRGD] = 3.3 μM and λ_{ex} = 360 nm for (A–F); [caspase-3] = 80 ng mL^{-1} for (B and E); [inhibitor] = 10 μM for (B).

maintain the complete fluorescence "off" state. On the other hand, when the probe is internalized into apoptotic cancer cells or healthy cancer cells upon drug induced apoptosis, the activated caspase enzymes should specifically cleave the Ac-DEVD moiety from the probe, leading to the release of TPS-cRGD. The amphiphilic TPS-cRGD molecules will subsequently turn on their fluorescence upon binding to cell components or form nanoaggregates *in situ* due to the RIR. These intermolecular interactions also help to retain the AIE probes inside the cancer cells, which afford good contrast for the real-time imaging of apoptotic progress.

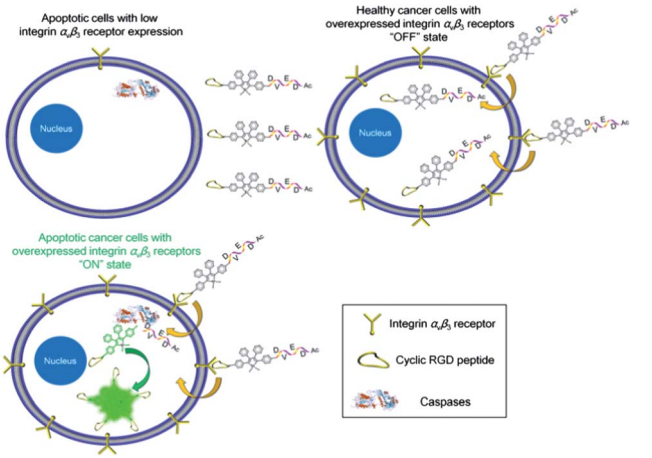

Scheme 2 The principle of apoptosis imaging in target cancer cell based on Ac-DEVD-TPS-cRGD.

To test our hypothesis, *in vitro* enzymatic assays with recombinant caspase-3, one of the key mediators of cell apoptosis in the caspase family,[18] were first carried out. Caspase-3 (80 ng mL^{-1}) was mixed with Ac-DEVD-TPS-N_3 (3.3 μM) or Ac-DEVD-TPS-cRGD (3.3 μM) in piperazine-*N*,*N*′-bis(2-ethanesulfonic acid) (PIPES) buffer (pH = 7.2), which was then incubated at 37 °C for 30 min. The corresponding PL spectra are shown in Fig. 1B. High fluorescent signals ranging from 400 to 650 nm are observed for both probes upon treatment with caspase-3. Moreover, most of the fluorescence cannot be observed by pretreatment of the two probes with 5-[(*S*)-(+)-2-(methoxymethyl)pyrrolidino] sulfonylisatin, a highly specific inhibitor for caspase-3.[19] The caspase-3-catalyzed hydrolysis of Ac-DEVD-TPS-cRGD was further verified by LC-MS (Fig. S7 in ESI†), which confirms that the fluorescence turn-on is through the specific cleavage of Ac-DEVD from the probe by caspase-3. It is noteworthy that the fluorescence intensity of the residual TPS-cRGD nanoaggregates (average diameter of ~43 nm, Fig. S8A and S8B in ESI†, Φ = 11% in water) is about 70% of that of the TPS-N_3 nanoaggregates (average diameter of ~94 nm, Fig. S8C in ESI†), because the cRGD peptide is hydrophilic, and as a consequence the TPS-cRGD fragment is more hydrophilic than TPS-N_3.

We next optimized the concentration of recombinant caspase-3 for the complete digestion of Ac-DEVD-TPS-cRGD. Fig. 1C shows the PL spectra of Ac-DEVD-TPS-cRGD (3.3 μM) after incubation with the enzyme in the concentration range from 0 to 160 ng mL^{-1} in PIPES buffer at 37 °C for 30 min. With the increasing concentration of caspase-3, the probe emission gradually increases. A ~70-fold increase in solution fluorescence is observed when the probe is treated with 160 ng mL^{-1} of caspase-3, as compared to that of the probe alone. As the PL intensity of the probe is close to saturation upon treatment with 80 ng mL^{-1} of caspase-3, the condition is used for the following enzymatic experiments. In addition, the PL intensities of the probes after treatment with caspase-3 increase linearly when the enzyme concentration is in the range of 0 to 80 ng mL^{-1} (Fig. 1D), indicating the possible use of Ac-DEVD-TPS-cRGD for caspase-3 quantification.

Fig. 1E illustrates the enzyme kinetic study from monitoring the PL intensity variations of Ac-DEVD-TPS-cRGD (3.3 μM) upon incubation with recombinant caspase-3 (80 ng mL^{-1}) in PIPES buffer at 37 °C within a 30 min duration. After enzyme treatment, a significant increase in solution fluorescence over the background is observed over time. In comparison, no obvious fluorescence change is detected in the absence of caspase-3. These results also confirm the specific cleavage of Ac-DEVD-TPS-cRGD by caspase-3. In addition, to further demonstrate the probe selectivity, the same amount of Ac-DEVD-TPS-cRGD was treated with different proteins, including cathepsin B, lysozyme, pepsin, papsin, trypsin, bovine serum albumin (BSA), caspase-1 and caspase-7 under the same experimental conditions. As shown in Fig. 1F, caspase-3 and caspase-7 exhibit far larger changes in $(I - I_0)/I_0$, as compared to other proteins, revealing that Ac-DEVD-TPS-cRGD is a unique probe for the specific recognition of caspase-3/7.

Apoptosis imaging in live target cancer cells based on Ac-DEVD-TPS-cRGD was studied with confocal laser scanning microscopy (CLSM). U87MG human glioblastoma cells (integrin $\alpha_v\beta_3$ receptor overexpression), MCF-7 human breast cancer cells (low integrin $\alpha_v\beta_3$ receptor expression) and 293 T normal cells (low integrin $\alpha_v\beta_3$ receptor expression) were chosen to demonstrate the utility of Ac-DEVD-TPS-cRGD in the apoptosis imaging of target cancer cells.[20] After incubating the cells with the probe at 37 °C for 2 h, staurosporine (STS, 1 μM), a drug known for inducing cell apoptosis,[21] was added, and the cells were further incubated for 1 h before CLSM imaging. As shown in Fig. 2A–C, for the Ac-DEVD-TPS-cRGD-treated U87MG cancer cells, the cell apoptosis induced by STS can switch on the fluorescence within the cells and the fluorescent signals are significantly blocked when STS-induced U87MG cells are pretreated with the specific caspase inhibitor, 5-[(*S*)-(+)-2-(methoxymethyl)pyrrolidino] sulfonylisatin prior to probe incubation. These results substantiate that the specific recognition and cleavage of Ac-DEVD-TPS-cRGD by caspases occurs within live cancer cells. It is noteworthy that the fluorescence intensity of Ac-DEVD-TPS-cRGD in healthy U87MG cancer cells is negligible (Fig. 2A), thanks to the good water-solubility of the probe. After STS induced cell apoptosis, the activated caspase enzymes trigger the digestion of Ac-DEVD from the probe, and the amphiphilic TPS-cRGD residues (Fig. S7 in ESI†) light up in the cells. It is important to note that the fluorescence contrast between the images shown in Fig. 2A and B is very sharp, which clearly indicates that Ac-DEVD-TPS-cRGD is very sensitive to the apoptosis imaging of live target cancer cells with minimum background signal. In contrast, obvious green fluorescence is observed when healthy U87MG cancer cells were incubated with Ac-DEVD-TPS-N_3 (Fig. S9A in ESI†), which highlights the contribution of the cRGD conjugation in reducing the probe background signal in cells. The fluorescence change in Fig. S9B and S9C in the ESI† further confirms the function of the caspases and the inhibitor.

To demonstrate the targeting ability of Ac-DEVD-TPS-cRGD to integrin $\alpha_v\beta_3$ receptor overexpressing cancer cells, a set of cell experiments were conducted using U87MG cells as an example. After incubating the healthy U87MG cells with Ac-DEVD-TPS-N_3 and Ac-DEVD-TPS-cRGD at 37 °C for 2 h, respectively, the cells were lysed and the cell lysates were analyzed by HPLC. As shown in Fig. S10 in ESI,† both probes possess good stability in a cellular environment for 2 h and ~1.9-fold more Ac-DEVD-TPS-cRGD can be internalized into U87MG cells as compared to that for Ac-DEVD-TPS-N_3. This should be due to the specific interactions between cRGD in the probe and the integrin $\alpha_v\beta_3$ receptors on the U87MG cell membrane, which favor a more efficient cellular uptake of Ac-DEVD-TPS-cRGD. In addition, as compared to Ac-DEVD-TPS-cRGD-treated apoptotic U87MG cells (Fig. 2B), the blocking of integrin $\alpha_v\beta_3$ receptors on the U87MG cell membrane with free cRGD peptides leads to significantly reduced fluorescent signals after inducing the apoptosis (Fig. 2G). Quantitative study using Image Pro Plus software indicates that the average fluorescence intensity from

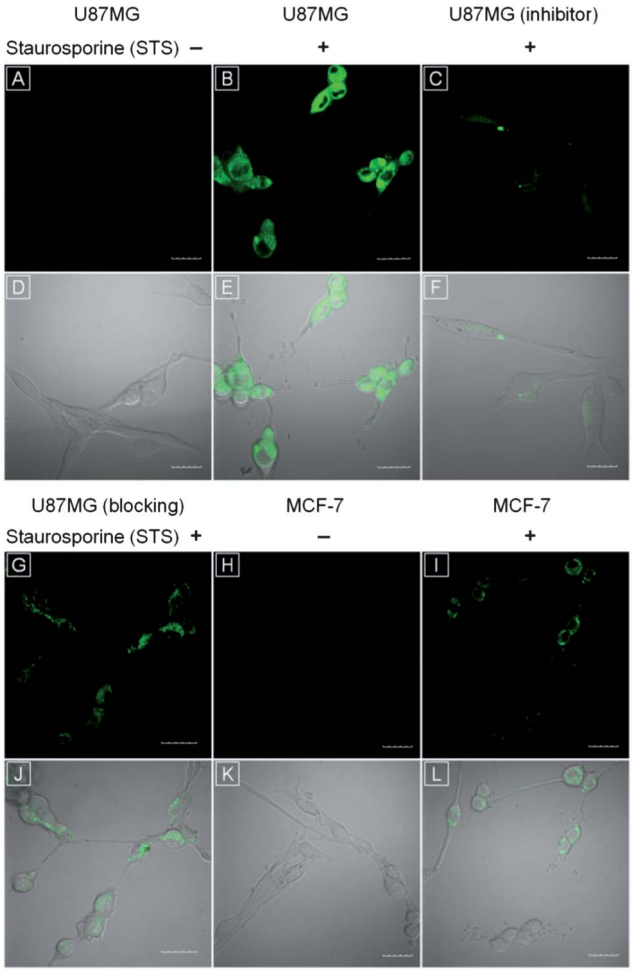

Fig. 2 CLSM images of healthy (A) and apoptotic U87MG cells (B) upon treatment with Ac-DEVD-TPS-cRGD; STS-induced U87MG cells pretreated with caspase inhibitor before Ac-DEVD-TPS-cRGD staining (C); U87MG cells pretreated with 10 μM cRGD followed by staining with Ac-DEVD-TPS-cRGD and STS induced cell apoptosis (G); healthy (H) and apoptotic MCF-7 cells (I) treated with Ac-DEVD-TPS-cRGD. (D–F) and (J–L) are the corresponding fluorescence/transmission overlay images of (A–C) and (G–I), respectively. [Ac-DEVD-TPS-cRGD] = 5 μM, [STS] = 1 μM, [inhibitor] = 10 μM. Scale bar: 30 μm for all the images.

each cell in Fig. 2B is ~1.8 times higher than that in Fig. 2G. These results manifest that the U87MG cell uptake of Ac-DEVD-TPS-cRGD is suppressed by free cRGD treatment, verifying that the cRGD peptide/integrin interaction promotes the probe internalization into U87MG cancer cells.

MCF-7 cells and 293 T cells with low integrin $\alpha_v\beta_3$ receptor expression were further utilized as controls to study the specific targeting ability of Ac-DEVD-TPS-cRGD to integrin $\alpha_v\beta_3$ receptor-overexpressing cancer cells. Fig. 2H and I show the Ac-DEVD-TPS-cRGD-stained MCF-7 cells before and after STS induced cell apoptosis, respectively. Almost no signal is detected in the Ac-DEVD-TPS-cRGD-treated healthy MCF-7 cells. Moreover, after STS induced cell apoptosis, although green fluorescence from Ac-DEVD-TPS-cRGD-treated apoptotic MCF-7 cells is observed, their intensities are ~2.2 times lower (analyzed by Image Pro Plus software) than that from the Ac-DEVD-TPS-cRGD-treated apoptotic U87MG cells (Fig. 2B). Similarly, low fluorescence is observed from Ac-DEVD-TPS-cRGD-treated apoptotic 293 T normal cells (Fig. S11 in ESI†). These results confirm the specific targeting ability of Ac-DEVD-TPS-cRGD to integrin $\alpha_v\beta_3$ receptor-overexpressing cancer cells, which not only favors apoptosis imaging in target cancer cells, but is also beneficial to achieving high contrast in imaging.

In addition, Ac-DEVD-TPS-cRGD-treated apoptotic U87MG cells were co-stained with commercially available Annexin V-Alexa Fluor 488 (ref. 22) and anti-caspase-3 primary antibody/Texas Red-labeled secondary antibody,[23] respectively. As shown in Fig. S12A–C in ESI,† the signal of Annexin V-Alexa Fluor 488 is observed on the cell surface, whereas Ac-DEVD-TPS-cRGD displays high fluorescence in the cytoplasma. Moreover, the green fluorescence from Ac-DEVD-TPS-cRGD and the red fluorescence from Texas Red co-localize well inside the cells (Fig. S12D–F in ESI†). This data clearly confirms that Ac-DEVD-TPS-cRGD is indeed an efficient and specific probe for the detection of caspase activity and apoptosis imaging in live cancer cells.

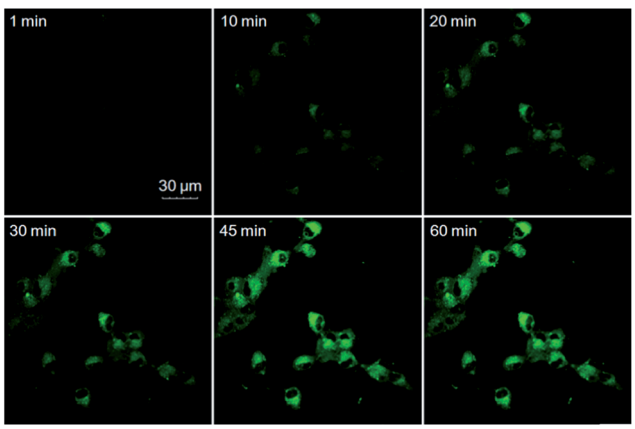

Fig. 3 Real-time CLSM images displaying the apoptotic progress of Ac-DEVD-TPS-cRGD-stained U87MG cells upon STS induced apoptosis at room temperature. [Ac-DEVD-TPS-cRGD] = 5 μM, [STS] = 1 μM. All images share the same scale bar.

To evaluate the capability of Ac-DEVD-TPS-cRGD in the real-time imaging of the apoptotic process in live cancer cells, U87MG cells were incubated with Ac-DEVD-TPS-cRGD at 37 °C for 2 h. After the cells were further treated with STS, they were immediately imaged by CLSM. Fig. 3 displays the real-time CLSM images recorded within a 1 h duration. The fluorescence intensity inside the U87MG cells gradually increases over time along with the cellular apoptotic progress, and the saturation is observed at 45 min. These results substantiate that Ac-DEVD-TPS-cRGD can serve as an effective light-up probe for the real-time imaging of cancer cell apoptosis. Additionally, the low cytotoxicity of Ac-DEVD-TPS-cRGD has also been demonstrated, which makes it a safe probe for bioimaging applications (Fig. S13 in ESI†).

4 Conclusions

In summary, we developed an asymmetric AIE bioprobe by the conjugation of Ac-DEVD and cRGD peptides onto a TPS luminogen. Opposite to the high fluorescence of azide functionalized TPS aggregates in aqueous media, the probe of Ac-DEVD-TPS-cRGD is dissolved as molecular species with almost no emission in aqueous solution. Thanks to the AIE feature of the TPS-cRGD resides, the probe is able to turn on its fluorescence when the activated caspases cleave the Ac-DEVD peptide from the probe. Cancer cellular apoptosis imaging studies, using integrin $\alpha_v\beta_3$ receptor-overexpressed U87MG cancer cells as an example, demonstrate that Ac-DEVD-TPS-cRGD has a specific targeting ability to U87MG cancer cells and can serve as a safe and efficient fluorescent light-up probe for real-time apoptosis imaging. This, in combination with the lower background signal of the probe to that of the Ac-DEVD-TPS-N_3, reveals the dual functions that the cRGD played in the probe design, namely, the targeting effect and higher contrast or improved sensitivity by providing a low background signal.

Acknowledgements

We thank the Singapore National Research Foundation (R-279-000-390-281), Singapore-MIT Alliance for Research and Technology (SMART) Innovation Grant (R279-000-378-592), the Institute of Materials Research and Engineering of A-star, Singapore (IMRE12-8P1103), the Research Grants Council of Hong Kong (HKUST2/CRF/10and N_HKUST620/11), and Guangdong Innovative Research Team Program of China (20110C0105067115) for financial support.

Notes and references

1 D. L. Vaux and S. J. Korsmeyer, *Cell*, 1999, **96**, 245.
2 (*a*) D. Hanahan and R. A. Weinberg, *Cell*, 2000, **100**, 57; (*b*) S. J. Riedl and Y. Shi, *Nat. Rev. Mol. Cell Biol.*, 2004, **5**, 897; (*c*) S. Lee, K. Y. Choi, H. Chung, J. H. Ryu, A. Lee, H. Koo, I. C. Youn, J. H. Park, I. S. Kim, S. Y. Kim, X. Y. Chen, S. Y. Jeong, I. C. Kwon, K. Kim and K. Choi, *Bioconjugate Chem.*, 2011, **22**, 125.

3 S. A. McKinney, C. S. Murphy, K. L. Hazelwood, M. W. Davidson and L. L. Looger, *Nat. Methods*, 2009, **6**, 131.
4 (*a*) H. Enright, R. P. Hebbel and K. A. Nath, *J. Lab. Clin. Med.*, 1994, **124**, 63; (*b*) F. G. Blankenberg, P. D. Katsikis, J. F. Tait, R. E. Davis, L. Naumovski, K. Ohtsuki, S. Kopiwoda, M. J. Abrams, M. Darkes, R. C. Robbins, H. T. Maecker and H. W. Strauss, *Proc. Natl. Acad. Sci. U. S. A.*, 1998, **95**, 6349; (*c*) L. Quiti, R. Weissleder and C. H. Tung, *Nano Lett.*, 2006, **6**, 488; (*d*) Z. Liu, K. Chen, C. Davis, S. Sherlock, Q. Z. Cao, X. Y. Chen and H. J. Dai, *Cancer Res.*, 2008, **68**, 6652.
5 S. L. Diamond, *Curr. Opin. Chem. Biol.*, 2007, **11**, 46.
6 T. Nagai and A. Miyawaki, *Biochem. Biophys. Res. Commun.*, 2004, **319**, 72.
7 J. F. Lovell, M. W. Chan, Q. C. Qi, J. Chen and G. Zheng, *J. Am. Chem. Soc.*, 2011, **133**, 18580.
8 (*a*) K. Kim, M. Lee, H. Park, J. H. Kim, S. Kim, H. Chung, K. Choi, I. S. Kim, B. L. Seong and I. C. Kwon, *J. Am. Chem. Soc.*, 2006, **128**, 3490; (*b*) K. Boeneman, B. C. Mei, A. M. Dennis, G. Bao, J. R. Deschamps, H. Mattoussi and I. L. Medintz, *J. Am. Chem. Soc.*, 2009, **131**, 3828; (*c*) S. Y. Lin, N. T. Chen, S. P. Sun, J. C. Chang, Y. C. Wang, C. S. Yang and L. W. Lo, *J. Am. Chem. Soc.*, 2010, **132**, 8309; (*d*) X. L. Huang, M. Swierczewska, K. Y. Choi, L. Zhu, A. Bhirde, J. W. Park, K. Kim, J. Xie, G. Niu, K. C. Lee, S. Lee and X. Y. Chen, *Angew. Chem., Int. Ed.*, 2012, **51**, 1625.
9 A. Kanno, Y. Yamanaka, H. Hirano, Y. Umezawa and T. Ozawa, *Angew. Chem., Int. Ed.*, 2007, **46**, 7595.
10 (*a*) S. H. Choi, I. C. Kwon, K. Y. Hwang, I. S. Kim and H. J. Ahn, *Biomacromolecules*, 2011, **12**, 3099; (*b*) W. Cao, L. Ji, G. Cui, K. Xu, P. Li and B. Tang, *Biomaterials*, 2012, **33**, 3710.
11 (*a*) J. D. Luo, Z. L. Xie, J. W. Y. Lam, L. Cheng, H. Y. Chen, C. F. Qiu, H. S. Kwok, X. W. Zhan, Y. Q. Liu, D. B. Zhu and B. Z. Tang, *Chem. Commun.*, 2001, 1740; (*b*) Z. Zhao, J. W. Y. Lam and B. Z. Tang, *Curr. Org. Chem.*, 2010, **14**, 2109; (*c*) Y. Liu, C. Deng, L. Tang, A. Qin, R. Hu, J. Z. Sun and B. Z. Tang, *J. Am. Chem. Soc.*, 2011, **133**, 660; (*d*) W. Qin, D. Ding, J. Z. Liu, W. Z. Yuan, Y. Hu, B. Liu and B. Z. Tang, *Adv. Funct. Mater.*, 2012, **22**, 771.
12 (*a*) Y. N. Hong, J. W. Y. Lam and B. Z. Tang, *Chem. Commun.*, 2009, 4332; (*b*) Y. N. Hong, J. W. Y. Lam and B. Z. Tang, *Chem. Soc. Rev.*, 2011, **40**, 5361.
13 (*a*) M. Wang, G. X. Zhang, D. Q. Zhang, D. B. Zhu and B. Z. Tang, *J. Mater. Chem.*, 2010, **20**, 1858; (*b*) Y. Liu, Y. Tang, N. N. Barashkov, I. S. Irgibaeva, J. W. Y. Lam, R. Hu, D. Birimzhanova, Y. Yu and B. Z. Tang, *J. Am. Chem. Soc.*, 2010, **132**, 13951; (*c*) Y. N. Hong, J. W. Y. Lam, S. J. Chen and B. Z. Tang, *Aust. J. Chem.*, 2011, **64**, 1203; (*d*) K. Li, W. Qin, D. Ding, N. Tomczak, J. L. Geng, R. R. Liu, J. Z. Liu, X. H. Zhang, H. W. Liu, B. Liu and B. Z. Tang, *Sci. Rep.*, 2013, **3**, 1150.
14 (*a*) H. B. Shi, J. Z. Liu, J. L. Geng, B. Z. Tang and B. Liu, *J. Am. Chem. Soc.*, 2012, **134**, 9569; (*b*) H. B. Shi, R. T. K. Kwok, J. Z. Liu, B. G. Xing, B. Z. Tang and B. Liu, *J. Am. Chem. Soc.*, 2012, **134**, 17972.
15 (*a*) X. Y. Chen, P. S. Conti and R. A. Moats, *Cancer Res.*, 2004, **64**, 8009; (*b*) Z. Cheng, Y. Wu, Z. Xiong, S. Gambhir and X. Y. Chen, *Bioconjugate Chem.*, 2005, **16**, 1433; (*c*) M. H. Lee, J. Y. Kim, J. H. Han, S. Bhuniya, J. L. Sessler, C. Kang and J. S. Kim, *J. Am. Chem. Soc.*, 2012, **134**, 12668.
16 S. Nagata, *Cell*, 1997, **88**, 355.
17 W. H. Melhuish, *J. Phys. Chem.*, 1961, **65**, 229.
18 A. G. Porter and R. U. Jäniche, *Cell Death Differ.*, 1999, **6**, 99.
19 J. Wang, X. Xiao, Y. Zhang, D. Shi, W. Chen, L. Fu, L. Liu, F. Xie, T. Kang, W. Huang and W. Deng, *J. Pineal Res.*, 2012, **53**, 77.
20 (*a*) H. Hong, J. Shi, Y. Yang, Y. Zhang, J. W. Engle, R. J. Nickles, X. Wang and W. Cai, *Nano Lett.*, 2011, **11**, 3744; (*b*) M. Oba, S. Fukushima, N. Kanayama, K. Aoyagi, N. Nishiyama, H. Koyama and K. Kataoka, *Bioconjugate Chem.*, 2007, **18**, 1415.
21 A. Lührmann, C. V. Nogueira, K. L. Carey and C. R. Roy, *Proc. Natl. Acad. Sci. U. S. A.*, 2010, **107**, 18997.
22 A. Lorents, P. K. Kodavali, N. Oskolkov, Ü. Langel, M. Hällbrink and M. Pooga, *J. Biol. Chem.*, 2012, **287**, 16880.
23 Q. Chang, I. Jurisica, T. Do and D. W. Hedley, *Cancer Res.*, 2011, **71**, 3110.

